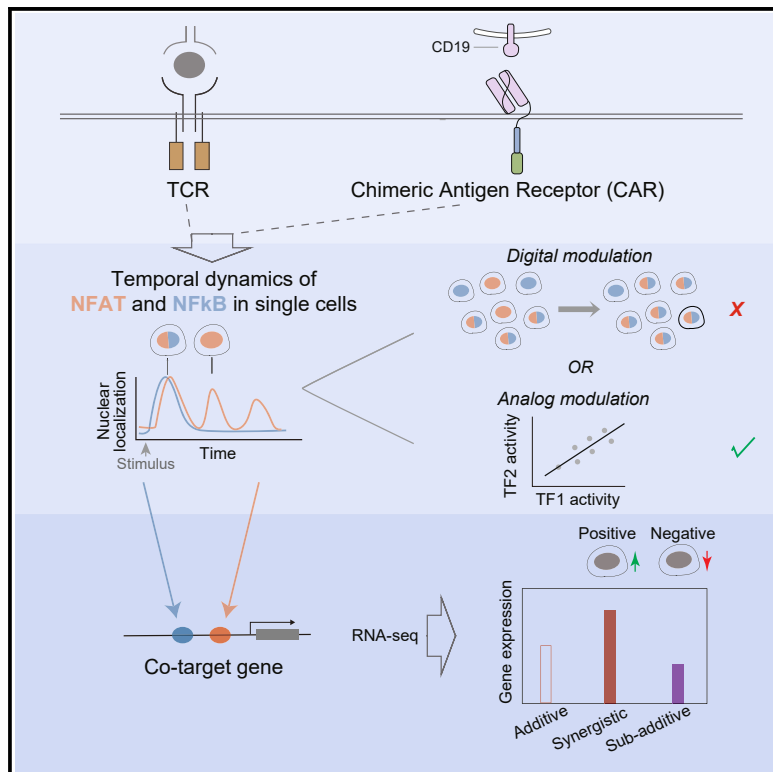


NFAT and NF- κ B dynamically co-regulate TCR and CAR signaling responses in human T cells

Graphical abstract



Authors

Wen Huang, Wei Lin, Baoqiang Chen, ..., Yingying Fan, Yihan Lin, Ping Wei

Correspondence

yihan.lin@pku.edu.cn (Y.L.), ping.wei@siat.ac.cn (P.W.)

In brief

Huang et al. show that the temporal relationships between the nuclear localization dynamics of NFAT and NF- κ B are modulated by signal strength and type during TCR or CAR signaling in human T cells. The temporal relationships between two regulator dynamics are decoded to tune the expression of immune response genes.

Highlights

- Single-cell analysis of dynamic TCR and CAR signaling responses in human T cells
- Temporal relationships between NFAT and NF- κ B are modulated in an analog mode
- Co-target genes with different functions decode temporal relationships differently
- TCR and CAR signaling responses share similar dynamic regulatory principles



Article

NFAT and NF-κB dynamically co-regulate TCR and CAR signaling responses in human T cells

Wen Huang,^{1,2} Wei Lin,^{1,2} Baoqiang Chen,^{1,2,3} Jianhan Zhang,^{1,2} Peifen Gao,¹ Yingying Fan,^{1,4} Yihan Lin,^{1,2,5,*} and Ping Wei^{1,4,*}

¹Center for Quantitative Biology and Peking-Tsinghua Center for Life Sciences, Academy for Advanced Interdisciplinary Studies, Peking University, Beijing 100871, China

²The MOE Key Laboratory of Cell Proliferation and Differentiation, School of Life Sciences, Peking University, Beijing 100871, China

³School of Life Sciences, Tsinghua University, Beijing 100084, China

⁴Center for Cell and Gene Circuit Design, CAS Key Laboratory of Quantitative Engineering Biology, Shenzhen Institute of Synthetic Biology, Shenzhen Institute of Advanced Technology, Chinese Academy of Sciences, Shenzhen 518055, China

⁵Lead contact

*Correspondence: yihan.lin@pku.edu.cn (Y.L.), ping.wei@siat.ac.cn (P.W.)

<https://doi.org/10.1016/j.celrep.2023.112663>

SUMMARY

While it has been established that the responses of T cells to antigens are combinatorially regulated by multiple signaling pathways, it remains elusive what mechanisms cells utilize to quantitatively modulate T cell responses during pathway integration. Here, we show that two key pathways in T cell signaling, calcium/nuclear factor of activated T cells (NFAT) and protein kinase C (PKC)/nuclear factor κB (NF-κB), integrate through a dynamic and combinatorial strategy to fine-tune T cell response genes. At the *cis*-regulatory level, the two pathways integrate through co-binding of NFAT and NF-κB to immune response genes. Pathway integration is further regulated temporally, where T cell receptor (TCR) and chimeric antigen receptor (CAR) activation signals modulate the temporal relationships between the nuclear localization dynamics of NFAT and NF-κB. Such physical and temporal integrations together contribute to distinct modes of expression modulation for genes. Thus, the temporal relationships between regulators can be modulated to affect their co-targets during immune responses, underscoring the importance of dynamic combinatorial regulation in cellular signaling.

INTRODUCTION

In response to antigens, T cells are activated to express immune response genes, including cytokines and differentiation factors.^{1,2} T cell activation is regulated by a complex signaling system that implements a series of mechanisms to quantitatively modulate signaling responses, beginning with specific antigen recognition mediated by T cell receptors (TCRs) and the cooperative assembly of signaling hubs facilitated by co-stimulatory signals.³ Phospho-signals emerged from the signaling hubs would then be propagated through a cascade of signaling molecules, including ZAP-70 and linker for activation of T cells (LAT), leading to production of three second messengers, IP3 (inositol triphosphate), diacylglycerol (DAG), and Ca²⁺. As a consequence, multiple signaling pathways are activated, with the calcium signal activating the transcription factor (TF) NFAT (nuclear factor of activated T cells) and the DAG signal activating AP-1 and NF-κB (nuclear factor κ-B) through two kinase signal pathways involving Ras and protein kinase Cθ (PKCθ).^{4–6} Although terminal TFs of calcium and kinase signaling pathways have been extensively studied for their gene-regulatory roles in T cell activation,^{1–3} the mechanisms these pathways implement to quantitatively and combinatorially regulate immune response

genes remain elusive (Figure S1A). It is also unclear whether the mechanisms for natural receptor signaling would apply to signaling through chimeric antigen receptors (CARs).^{7–10} Addressing these questions would not only extend our understanding of T cell signaling but also provide guiding principles for the design of synthetic receptors for therapeutic applications.

A comprehensive dissection of how combinatorial gene regulation mediates T cell responses would require examining such a strategy at multiple levels. First, because each TF often has tens and hundreds of target genes,^{11–13} different TFs could share overlapping targets just by chance (i.e., passive). Thus, if cells “actively” implement a combinatorial strategy using multiple TFs, then these TFs would tend to actively, instead of passively, share overlapping targets, as if TFs were physically wired together to co-regulate genes. In addition to interactions at the physical level, it would also be necessary to examine the temporal relationships between TFs.^{14–18} This is because many TFs are known to display distinct temporal activity dynamics in response to different stimuli,^{15,19} and such dynamics can determine the specificity and level of target gene expression.^{20–25} We and others have demonstrated that TFs that share the same targets can combinatorially regulate genes by modulating their temporal relationships^{14,17,26} instead of changing the levels of their



activities, adding further challenges for understanding combinatorial gene regulation. Because immune-related signaling pathways, including calcium/NFAT and PKC/NF- κ B, are known to behave dynamically,^{16,25,27–29} where terminal TFs display different temporal activity patterns in response to different stimuli, it would be necessary to examine whether and how such TFs combinatorially regulate target genes in a temporal manner.¹⁵ Additionally, at the level of the promoter, it is necessary to analyze the quantitative dependence of target gene output on the activity levels of multiple TFs, which would allow discerning the specificity and mode of combinatorial regulation.³⁰

Here, we quantitatively dissected the role of combined activation of the calcium/NFAT and PKC/NF- κ B pathways during TCR and CAR signaling in human T cells. At the physical interaction level, we found that, among all possible pairs of TFs, NFAT and NF- κ B are highly ranked in terms of their “physical wiring” strength at *cis*-regulatory regions. At the temporal interaction level, we showed that their temporal relationships are modulated by TCR or anti-CD19 CAR activation in a stimulus strength- or co-stimulatory signal-dependent manner. Furthermore, we identified immune response genes that are synergistically activated when both TFs are temporally co-localizing in the nucleus. Collectively, we delineated the potential mechanisms implemented during the integration of two T cell signaling pathways at the level of terminal TFs and demonstrated how quantitative principles identified in TCR signaling are shared by CAR signaling, which could provide guidance for the future development of synthetic receptors for T cell-based therapy.

RESULTS

Pathway integration through active co-binding of NFAT and NF- κ B to T cell activation genes

To study the integration of the calcium/NFAT and PKC/NF- κ B pathways at the level of target gene regulation, we needed to quantitatively delineate the mechanisms that cells implement to enable combinatorial gene regulation by terminal TFs, NFAT and NF- κ B. For a gene to be combinatorially regulated by NFAT and NF- κ B, two mechanisms should be implemented: (1) the *cis*-regulatory region of the gene should contain binding sites for both TFs, and (2) the two TFs should temporally bind to and interact on the *cis*-regulatory region of the gene. Therefore, even when a target gene contains binding sites for two TFs, it might not be combinatorially regulated if the two TFs are not co-expressed or not both activated. Thus, we asked whether NFAT and NF- κ B can physically co-bind to T cell response genes and whether and how they are temporally interacting to co-regulate these genes.

To study physical co-binding, we need to discern between active versus passive modes of co-binding by NFAT and NF- κ B. That is, whether the probability of having two TFs’ binding sites on the *cis*-regulatory region of the same target is above random occurrence because two TFs could, by chance, share the same targets. Thus, we resorted to public chromatin immunoprecipitation sequencing (ChIP-seq) datasets summarized by ChIP-Atlas, where we extracted the inferred target genes bound by either NFAT or NF- κ B in T cells.³¹ Because NFAT ChIP-seq data are only available in human CD4+ T cells

(including Th1 cells), we focused on this cell type. We found that NFAT and NF- κ B (including all isoforms) have 1,821 and 9,526 inferred target genes, respectively, and that, among these genes, 1,550 targets are shared (Table S1). At the isoform level, NFAT1 and RELA share 1,531 targets, while NFAT2 and RELA share 142 targets. To test whether the occurrence of the shared targets is beyond random, we calculated the hypergeometric p value as well as the fold change between the number of actual and random co-binding targets. We found that NFAT and NF- κ B are statistically enriched for co-binding events ($-\log p = 912.3$) (Figure S1B), with the observed-to-random fold change being about 2-fold (Figure S1C). Gene Ontology analysis revealed that these co-binding genes are enriched for “regulation of T cell activation” (Figure S1D), as exemplified by IL-2RA (interleukin-2 receptor subunit alpha) and CD27 (a costimulatory molecule for T cell activation), while the single targets are enriched for analogous terms (Figure S1E). We further found that the number of co-binding targets between NFAT and NF- κ B ranks in the top 12% among all possible TFs analyzed with ChIP-seq data in CD4+ T cells (Figures S1F and S1G).

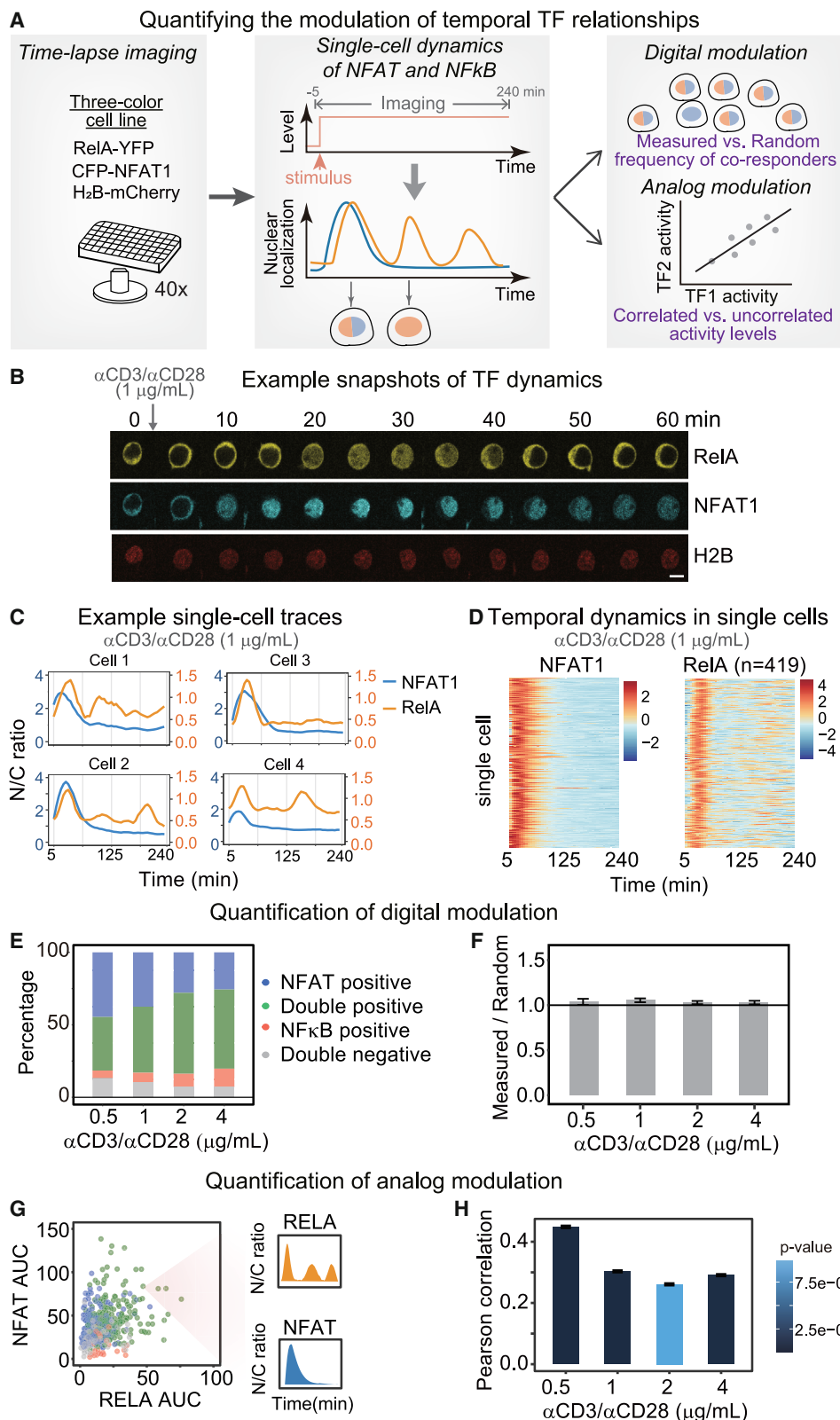
These results are consistent with the picture that, at the *cis*-regulatory level, an active, rather than passive, strategy is implemented by T cells to “physically wire” the two TFs onto the same *cis*-regulatory regions that regulate essential T cell response genes.

Pathway integration through active modulation of temporal relationships between NFAT and NF- κ B during TCR signaling

While NFAT and NF- κ B display a significant co-binding capability, it is necessary to investigate whether and how the two TFs are indeed activated in the same single cells. In other words, co-binding targets in a specific cell would not be combinatorially regulated by NFAT and NF- κ B if only one TF is activated in this cell; i.e., there are no temporal interactions between the two TFs.^{14,17} Thus, we next focused on analyzing their temporal relationships at the single-cell level in response to different stimuli (Figure 1A). Note that we focused on studying the responses to a step change in an external stimulus, where the stimulus strength abruptly transits to a predetermined level and is subsequently maintained for the duration of the study (Figure 1A, center).

We first developed a two-color time-lapse imaging assay for quantifying the single-cell activation dynamics of NFAT and NF- κ B. To do so, we constructed a monoclonal cell line with exogenously expressed TFs that are fluorescently labeled (cyan fluorescent protein mTurquoise2 [CFP]-NFAT1 and RelA-yellow fluorescent protein mCitrine [YFP]), together with a nucleus labeling marker (H2B-infrared red fluorescent protein [iRFP]), in Jurkat T cells. It has been demonstrated previously that exogenous expression of NFAT1 and RelA can still capture the responses of wild-type cells.^{6,16,25,28,32,33} We then performed live-cell imaging on this cell line to quantify the nuclear translocation dynamics of TFs in response to TCR activation by anti-CD3 and anti-CD28 antibodies (abbreviated as α CD3/ α CD28) (Figure 1B; Video S1).

The data revealed several notable differences between the dynamics of the two TFs. First, NFAT showed an adaptive



(legend on next page)

transient response (i.e., returning to close to basal levels after a burst of activity) while NF- κ B exhibited dampened oscillation-like dynamics (Figures 1C and 1D). The observed dynamics are qualitatively similar to findings from earlier studies on these two TFs in other cell types.^{16,25} The different response dynamics may come from the different mechanisms regulating the TF activities. NFAT nuclear translocation is triggered by rapidly elevated calcineurin activity following TCR activation and is then inhibited by the phosphatases DYRK (dual-specificity tyrosine-regulated kinases) and GSK3 (glycogen synthase kinase 3) and the NFAT negative feedback protein DSCR1 (desmocollin-1).^{34–36} The damped oscillation-like dynamics of NF- κ B likely arise from the negative feedback from multiple target genes, such as I κ B α and A20,^{29,37–39} which also occurs upon activation of B cell receptor (BCR), tumor necrosis factor receptor (TNFR), and Toll-like receptor (TLR).⁴⁰ Importantly, characteristics of the dynamics of NFAT remained relatively invariant to the stimulus strength (Figures S2A and S2B), while the dynamics of NF- κ B were modulated by stimulus strength, such as the responding cell fraction, peak amplitude, and fraction of cells with a second pulse (Figures S2C and S2D).

Second, we found that NFAT showed a quick response to the stimulus and fully translocated into the nucleus within 5–10 min, while NF- κ B responded after 15 min (Figure 1B). Such a delay between the two TFs' responses can be further quantified by the time lag in the cross-correlation function calculated using two TF dynamics in individual cells (Figure S2E; STAR Methods), showing a consistent, ~5-min delay across different levels of simulations. The time delay likely arises from the difference in the regulatory mechanisms. NFAT enters the nucleus by exposing the nuclear localization sequence through dephosphorylation by calcineurin.³⁴ In contrast, nuclear activation of NF- κ B involves a cascade of phosphorylation and ubiquitination reactions, including formation of the CARD11:Bcl10:MALT1 (CBM) complex, activation of I κ B kinase (IKK), and degradation of the inhibitory protein I κ B α .⁴¹

Third, NF- κ B dynamics exhibited a more pronounced single-cell heterogeneity. The single-cell trajectories showed that, across single cells, NFAT responded relatively consistently in response to TCR activation, with an intranuclear residence time of about 60 min, while the nuclear translocation dynamics of RelA exhibited asynchronous pulsatile dynamics after the first

activity pulse (Figures 1C, 1D, and S2A). This suggests that NFAT response is largely adaptive at the single-cell level and at the population level, while NF- κ B response is adaptive in a fraction of cells and displays repetitive activity pulses in other cells (Figure S2D). Such adaptive behavior suggests that the calcium/NFAT pathway is highly capable of adapting to changes in signaling inputs, allowing the cell to maintain a certain level of responsiveness to subsequent stimuli.

Having established that NFAT and NF- κ B exhibit different activity dynamics, we next focused on their activity relationships under different TCR stimulations in individual cells. Because of the dynamic responses of the two TFs, their activity relationships could be modulated either in a digital (or binary) manner by regulating the fraction of cells with both TFs activated or in an analog manner by influencing the correlation between the activity levels of the TFs when both are activated (Figure 1A, right). Note that we use “passive” regulation to describe changes in the temporal relationships between the two TFs that can arise from changes in each TF. As an example, if we increase the pulse frequency of each TF, then we would naturally observe more events of co-pulsing of the two TFs, simply because of the increased probability of two TFs being activated at the same time. In contrast, we used “active” to describe changes in the temporal relationships that cannot be explained by the changes in individual TFs alone.

To characterize digital modulation, because co-activation of two TFs could occur passively by chance (i.e., independent activation of each TF), we calculated the ratio between the measured fraction of cells with both TFs activated versus the “random” fraction of cells with both TFs activated (i.e., by assuming independence) under each condition (Figures 1E and 1F; see STAR Methods for details). For analog modulation, we calculated the correlation between their activities in individual cells (Figures 1G, 1H, and S2F). Intriguingly, we found evidence of analog modulation because the correlation of the areas under the curve (AUCs) between two TFs is statistically significant, and the strength of analog modulation (quantified by the degree of correlation of AUCs) decreases as stimulation enhances (Figure 1H). However, no evidence was found of digital modulation (Figure 1F) because the measured co-activation fraction is almost equal to the expected (i.e., random) co-activation fraction. That is, cells appeared to “actively” increase the correlation

Figure 1. Pathway integration through active modulation of NFAT and NF- κ B dynamics during TCR signaling

- (A) Quantifying the modulation of temporal TF relationships. Single-cell dynamics of NFAT and NF- κ B are important for identifying the two potential modes of temporal modulation; i.e., digital modulation and analog modulation.
- (B) Assay for quantifying dynamic single-cell responses. Three-color snapshots show an example cell stimulated by α CD3/ α CD28 antibodies (1 μ g/mL), which was added at $t = 0$ h and maintained throughout the experimental time course. The scale bar indicates 10 μ m.
- (C and D) Example single-cell traces of TF dynamics (C) and heatmaps of the TF dynamics of all single cells (D) under the stimulation of α CD3/ α CD28 antibodies (1 μ g/mL, $n = 419$). In (D), each row indicates a cell, and color indicates scaled TF localization level.
- (E and F) Quantification of digital modulation. The activation (responder) ratios were characterized under various concentrations of α CD3/ α CD28 antibodies (E). The ratios between the measured fraction and the “random” fraction of cells with both TFs activated were calculated (F) (STAR Methods). Error bars indicate 95% confidence interval (CI) from bootstrap. $n = 314, 419, 425$, and 419 cells from left to right.
- (G and H) Quantification of analog modulation. The NFAT and NF- κ B activity levels were estimated using areas under the curve (AUCs), which were extracted from single-cell nuclear translocation dynamics (i.e., 4-h trajectories post stimulation) (G). Pearson correlations between NFAT and NF- κ B activity levels in individual cells quantify the degrees of analog modulation under various concentrations of α CD3/ α CD28 antibodies (H). $n = 314, 419, 425$, and 419 cells from left to right. Error bars indicate 95% CI from bootstrap. p -values were calculated for association between paired samples using Pearson's product moment correlation coefficient.

See also Figures S1 and S2.

between the activity levels of TFs but not the probability of having both TFs activated in the same cell. These results indicate that, during TCR signaling, the two TFs are temporally co-activated in a passive manner (with each being activated independently), whereas their activity levels appear to be coordinated in an active manner.

Taken together, the two-color dynamic traces revealed how each TF's activity dynamics are modulated by TCR stimulation and, more importantly, suggested the presence of active modulation of their temporal relationships in an analog manner, with the degree of modulation unexpectedly decreasing as stimulus strength increased.

Modulation of temporal TF relationships is mediated by TCR-dependent and TCR-independent mechanisms

The findings above raise questions regarding the mechanisms underlying the modulation of the temporal relationships between NFAT and NF- κ B. We speculated that the observed analog modulation could arise from cross-regulation of the terminal TFs by upstream regulators and may not necessarily require the involvement of the TCR.

To explore this, we bypassed the TCR by leveraging two chemicals, PMA (phorbol-12-myristate-13-acetate) and ionomycin, which chemically mimic TCR activation by activating kinase pathways and calcium signaling, respectively.^{42,43} PMA is a DAG analog that activates PKC and its downstream mitogen-activated protein kinase (MAPK) and NF- κ B. Ionomycin is a highly selective calcium ion chelator and can transiently alter the intracellular Ca²⁺ level and release calcium storage in the endoplasmic reticulum, thereby activating the calcineurin-controlled NFAT (Figure 2A). Using a reporter assay, we validated the specific activation of NF- κ B by PMA and the specific activation of NFAT by ionomycin (Figure 2A). Temporally, NF- κ B was activated in a pulsatile manner (Figures 2B and 2C; Video S1), analogous to the response to TCR activation (Figure S2A), with the concentration of PMA modulating the amplitude and number of pulses as well as the fraction of responding cells (Figure S3A). In contrast, NFAT was activated in a sustained manner (Figures 2B and 2C), distinct from the response to TCR activation and potentially because of the sustained increase in Ca²⁺ level, with the concentration of ionomycin largely modulating the amplitude of the response and the fraction of responding cells (Figure S3B). The characteristics of the responses can also be visualized with heatmaps of single-cell dynamics (Figures S4A and S4B) and distributions of single-cell activity levels (Figures S4C and S4D). Note that, in Figure S3A, although Ca²⁺ signaling activation alone (via ionomycin treatment) could not drive NF- κ B into the nucleus, addition of PMA significantly enhanced the proportion of cells exhibiting NF- κ B responses and the intensity of these responses (Figures S3A and 2D). This enhancement can be partially attributed to the slight ability of ionomycin to activate PKC (which activates NF- κ B). Additionally, the effect of the calcium signal on proximal NF- κ B signaling (such as phosphorylation of NF- κ B protein) and distal NF- κ B signaling (assembly and activation of the upstream CBM complex) may also contribute to this observation.

Having established the capability to independently activate the two pathways without TCR involvement, we next studied

whether and how the combined action of the two chemicals would modulate temporal TF relationships, which could allow us to discern the role of the TCR in temporal modulation. We thus quantified the modulation of the temporal TF relationship for cells subjected to combined stimulation of PMA and ionomycin. We found no evidence supporting the presence of digital modulation (Figures 2D and 2E, left), analogous to the TCR activation condition. In comparison, the correlation between TF activity levels is statistically significant, indicating that PMA/ionomycin stimulation can also modulate the temporal TF relationship in an analog manner similar to the TCR activation condition, albeit to a smaller extent (Figure 2E, right).

Thus, even without the TCR, the temporal relationships between the two TFs could still be modulated in an analog manner, potentially mediated by cross-regulation downstream of DAG and IP3. More generally, this result suggested that pathway integration could be temporally modulated at multiple stages of the signaling system (i.e., at the stages of receptor activation and pathway cross-talk).

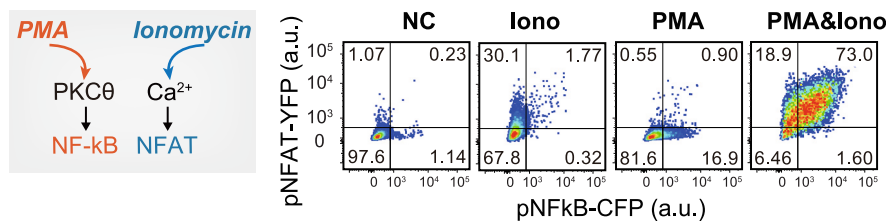
To further support the picture that the temporal interactions between the calcium/NFAT and PKC/NF- κ B pathways are modulated during TCR activation, we sought to perturb activation of the two pathways independent of TCR signaling and test whether temporal modulation by TCR signaling could be weakened or strengthened by perturbations targeting specific pathways. More specifically, we hypothesized that, if we specifically enhance activation of only one of the two pathways during TCR signaling, then the temporal modulation would be weakened.

To test this hypothesis, we resorted to ionomycin, which was able to specifically enhance NFAT activation by lengthening its pulse duration during TCR signaling (i.e., when cells were treated with both α CD3/ α CD28 antibodies and ionomycin) (Figures S5A and S5B). Under this condition, we found that the temporal relationship between two TFs was much weakened because the correlation between their activity levels was reduced and became less statistically significant (Figure 2F). This observation is consistent with the picture that ionomycin alters the temporal TF relationship by specifically tuning one but not the other TF, thus decoupling the two TFs.

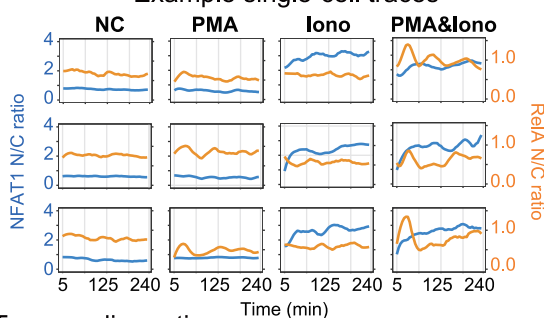
To further test the hypothesis, we sought to specifically perturb NF- κ B activation during TCR signaling by using PMA (Figures S5C and S5D). While PMA was unexpectedly found to also affect NFAT dynamics when combined with α CD3/ α CD28 antibodies (Figure S5C), we were able to isolate a subset of cells with perturbed NF- κ B activation whose NFAT dynamics are comparable with cells without PMA (with only α CD3/ α CD28 antibodies) (Figure S5D). For these cells, the correlation between the activation levels of NF- κ B and NFAT were absent (Figure 2F), which suggests that specific perturbation of NF- κ B activation disrupts the temporal relationship between NF- κ B and NFAT, effectively negating the temporal modulation by TCR activation.

Taken together, these results support the notion that the temporal relationships between the two TFs can be modulated by diverse inputs at different levels of the signaling pathway.

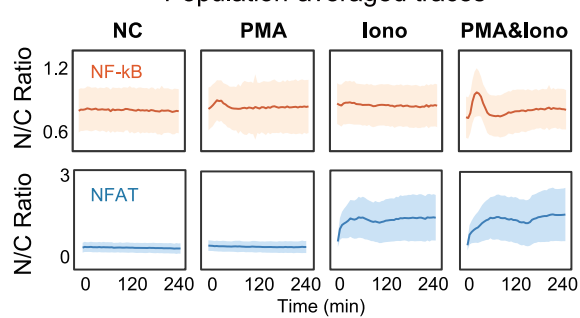
A Ionomycin and PMA for independent tuning of NFAT and NF- κ B



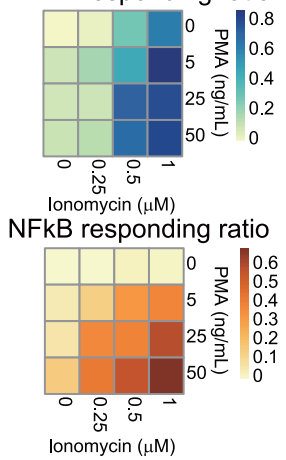
B Example single-cell traces



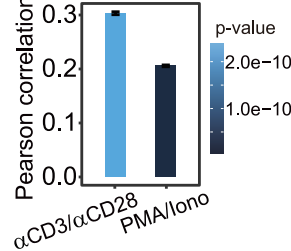
C Population-averaged traces



D NFAT responding ratio



E Quantification of digital and analog modulation



F Perturbation of analog modulation

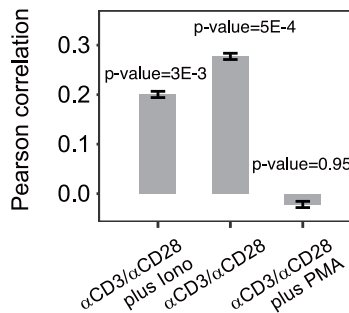


Figure 2. Modulation of temporal TF relationships is mediated by TCR-dependent and TCR-independent mechanisms

(A) The combination of PMA and ionomycin was used to bypass the TCR, which chemically mimics TCR activation by activating kinase pathways and calcium signaling, respectively (left). Flow cytometry results of promoter reporters illustrate the specific activation of NF- κ B or NFAT by PMA or ionomycin, respectively (right). PMA, 50 ng/mL; ionomycin, 1.0 μ M.

(B and C) Example single-cell (B) and population-averaged (C) nuclear translocation dynamics of NFAT and NF- κ B under the indicated stimulations. PMA, 50 ng/mL; ionomycin, 1.0 μ M. Shading indicates standard deviation, and centers indicate means. n = 61, 97, 69, and 101 cells from left to right.

(D) The activation (responder) ratios were characterized under various concentrations of PMA and ionomycin. n = 44–122 cells.

(E) Quantification of digital and analog modulation. The ratio between the measured fraction and the “random” fraction of cells with both TFs activated was calculated under PMA/ionomycin condition (50 ng/mL PMA and 1.0 μ M ionomycin, n = 101 cells) and was compared with the TCR activation condition (1 μ g/mL α CD3/ α CD28 antibodies, n = 419 cells) from Figure 1F (left). Analogous comparison was made for Pearson correlation between NFAT and NF- κ B activity levels (right). Error bars indicate 95% CI from bootstrap.

(F) Pearson correlations between the two TFs’ activity levels in individual cells when perturbing one but not the other signaling branch during TCR signaling. Perturbation of the NFAT branch was achieved by using ionomycin (0.6 μ M) during TCR activation by 1 μ g/mL antibodies (Figure S5A, n = 209 cells), while perturbation of the NF- κ B branch was achieved by using 1 ng/mL PMA (Figure S5C; n = 146 cells). Error bars indicate 95% CI from bootstrap. See also Figures S3–S5.

Modulation of temporal TF relationships by CAR signaling

In light of the current successes with immunotherapy using CAR-T cells,⁸ understanding the signaling mechanisms underlying

CAR-T cells is critical for continuous optimization of CAR design.^{44,45} The findings above prompted us to investigate whether the same dynamic combinatorial regulatory mechanism would also apply to T cell signaling through CARs. More

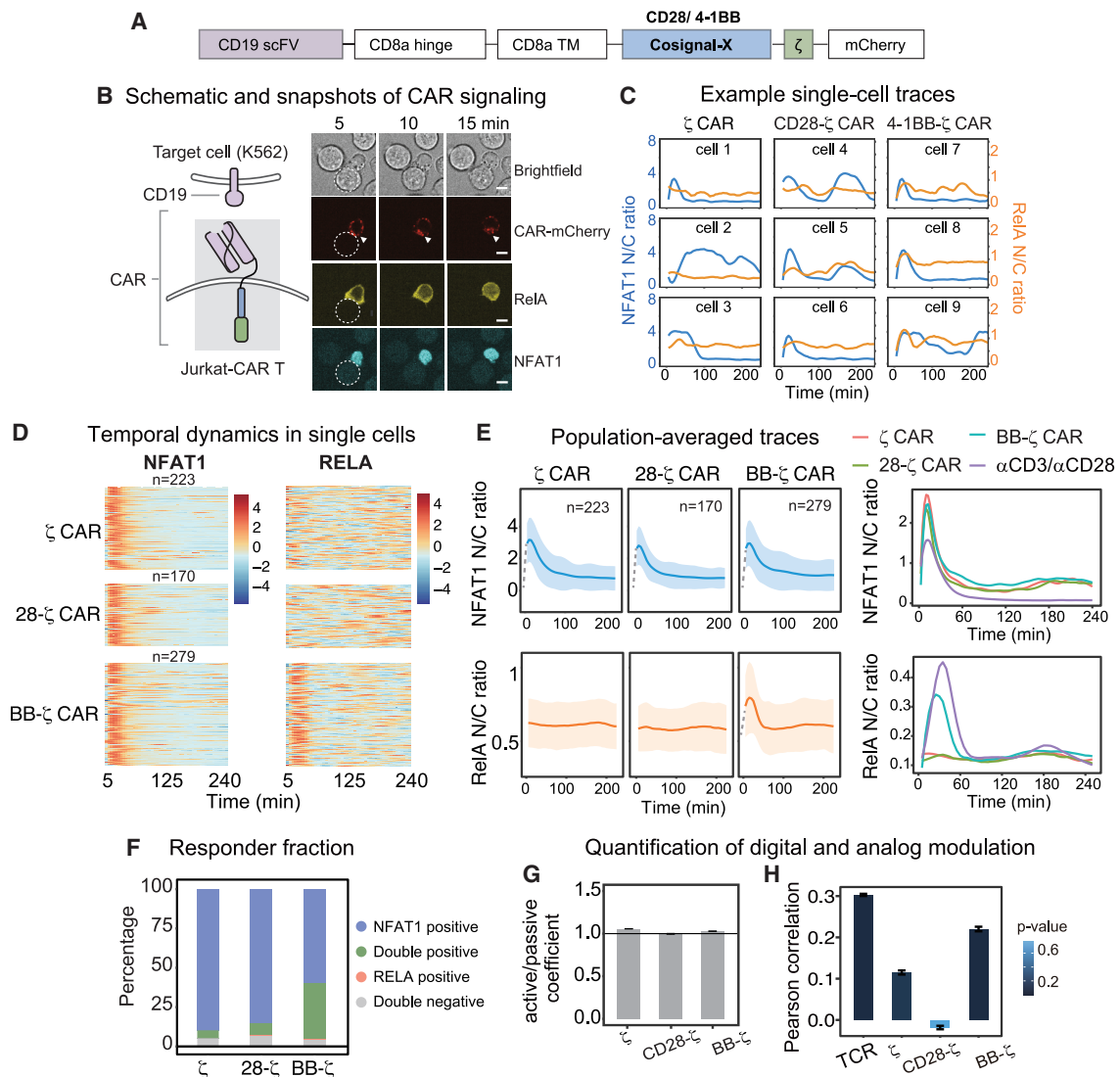


Figure 3. Modulation of temporal TF relationships by chimeric antigen receptor (CAR) signaling

(A) The design of three different CD19 CARs.

(B) Schematic and snapshots at the indicated time points post stimulation of an example cell (carrying the 4-1BB CAR) showing that the constructed CD19 Jurkat CAR-T cells can be activated by K562 target cells expressing CD19 antigen. The scale bar indicates 10 μ m.

(C and D) Example single-cell traces of NFAT and NF- κ B dynamics (C) and heatmaps of the TF dynamics in single cells (D) for the indicated Jurkat CAR-T cell line upon activation by K562 target cells expressing CD19 antigen. In (D), each row indicates a cell, and color indicates scaled TF localization level. n = 223, 170, and 279 cells from top to bottom.

(E) Population-averaged nuclear translocation dynamics of NFAT and NF- κ B for the indicated CAR-T cell line upon stimulation (left). These averaged traces were plotted together with traces from activation by 1 μ g/mL α CD3/ α CD28 antibodies (right). Shading indicates standard deviation, and centers indicate means. n = 223, 170, and 279 cells.

(F) The activation (responder) ratios were characterized for the indicated CAR-T cell line upon stimulation.

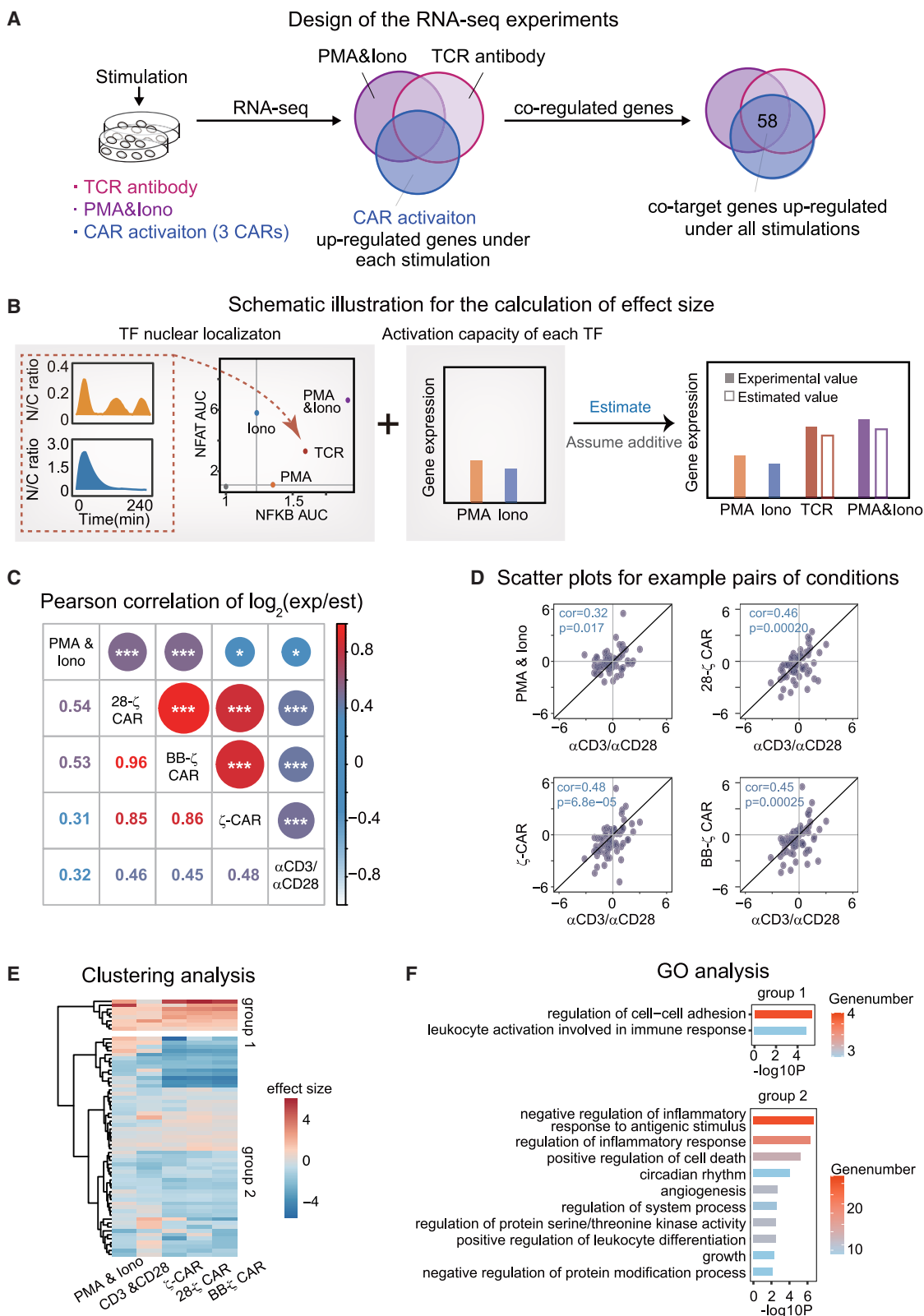
(G and H) Quantification of digital (G) and analog (H) modulation in CAR-T cell lines. "TCR" denotes the activation condition by 1 μ g/mL α CD3/ α CD28 antibodies (data from Figure 1H). Error bars indicate 95% CI by bootstrap.

See also Figure S6.

specifically, we sought to address whether and how CAR signaling modulates the temporal relationships between NFAT and NF- κ B.

We thus constructed three different CAR-T cell lines based on the two-color cell line constructed above, with each cell

line expressing CARs of different designs, including the first-generation CAR (i.e., ζ -CAR) and two different second-generation CARs fused with the intracellular segment of CD28 or 41BB (i.e., 28- ζ and BB- ζ CAR) (Figure 3A).⁴⁶ The constructed CARs share the same backbone structure and



(legend on next page)

extracellular anti-CD19 single-chain fragment variable (scFV), which can be activated by K562 cells expressing CD19 antigen. These CARs are also fused with mCherry to facilitate visualization of immunological synapses. By mixing CAR-T cells with K562 cells expressing CD19 antigen, we were able to observe clustering of CAR molecules in the immunological synapses and performed real-time monitoring of NFAT and NF- κ B nuclear translocation dynamics during CAR-T cell activation (Figure 3B; Video S2).

Across all three CAR-T cell lines, we found that NFAT was quickly activated upon contact with K562 cells (Figures 3C and 3D). Intriguingly, NFAT dynamics upon CAR activation exhibited much more variable single-cell dynamics compared with TCR activation, with cells displaying a transient response (analogous to TCR activation), sustained response (analogous to chemical analog stimulation), oscillatory response, or oscillation coupled with persistent activation (Figures 3C and 3D). This phenomenon potentially resulted from the variability in the number of contacts with target cells, as evidenced by bright-field imaging, which could lead to differential Ca^{2+} dynamics. To test this hypothesis, we imaged cells using a read calcium probe (Calbryte 590 AM) to monitor the Ca^{2+} signal under CAR activation. We found that cells could indeed excite multiple Ca^{2+} pulses, leading to sustained pulsing of NFAT dynamics, among other types of Ca^{2+} dynamics (Figures S6A–S6C). Consistent with this observation, Ca^{2+} dynamics under TCR activation or chemical analog stimulation display distinct characteristics that concord with the corresponding NFAT dynamics (Video S3). Intriguingly, the finding that all three CAR-T cell lines displayed similar NFAT dynamics (Figure 3E) implied that different designs of CARs possess comparable abilities to activate the calcium/NFAT pathway.

In contrast, NF- κ B dynamics upon CAR activation were highly variable across different CARs, with ζ -CAR displaying minimal NF- κ B activation and the BB- ζ CAR exhibiting the strongest NF- κ B activation (Figure 3E). At the single-cell level, NF- κ B translocation occurred approximately 10–20 min after contact with target cells and could display several activity pulses throughout the time course (Figures 3C and 3D). Such observed dynamics are analogous to the dynamics induced by TCR activation, implying that BB- ζ CAR elicits activation of the PKC/NF- κ B pathway comparable with the TCR (Figure 3E). Importantly, these results reassuringly validated that different CARs differ in their capabilities to activate NF- κ B as they were designed. More specifically, the distinct response characteristics of BB- ζ CAR are

likely related to the co-stimulatory structure because the TNFR superfamily (TNFRSF) receptor (such as CD27, OX40, and 4-1BB) can recruit TRAF (TNF-receptor-associated factor) family proteins,⁴⁰ promoting activation of IKK and NIK (NF- κ B-inducing kinase) and consequently activating the classical and non-classical NF- κ B pathways they mediate, respectively.

To test whether the observed TF dynamics during CAR signaling are specific to Jurkat cells, we constructed four-color reporter cell lines using primary human CD3+ T cells, which express CFP-NFAT1, RelA-YFP, H2B-iRFP, and one of the mCherry-fused CAR receptors. With these primary human T cells, we used time-lapse imaging to monitor TF dynamics upon CAR activation analogous to the Jurkat cell lines (Video S4). We found that, among all three CARs, NFAT was activated similarly in the primary cells to in the Jurkat cells (Figure S6D). For NF- κ B, it was weakly activated in ζ -CAR cells, and its activation strength was highest in BB- ζ CAR cells (Figure S6D), which were observed similarly to the Jurkat cells. Therefore, the temporal dynamics of the two TFs during CAR signaling are dependent on the type of CAR instead of the host cell type, underscoring the physiological relevance of using Jurkat cells for studying CAR signaling.

We next analyzed whether and how NFAT and NF- κ B temporally interact during T cell activation mediated by CAR signaling. We quantified the degree of digital and analog modulations. Among the three CARs, no evidence of digital modulation was found, as with other stimulations, and BB- ζ CAR appeared to modulate TF relationships in an analog manner (Figures S6E and 3F–3H), which is also evident from the reporter assay (Figure S6F). This finding suggested that, similar to TCR signaling, CAR signaling can modulate the extent of co-activation but not the probability of co-activation.

Physical and temporal pathway integration together contribute to differential gene regulation

Having established that the two pathways integrate physically and temporally during TCR and CAR signaling, we next asked how such integration influences target gene expression. To do so, we needed to measure the transcriptomic responses of T cells to diverse stimulations and analyze the quantitative effects of pathway integration on gene expression responses.

We thus used RNA sequencing (RNA-seq) to profile gene expression changes during α CD3/ α CD28-mediated TCR activation, PMA/ionomycin-mediated T cell activation, CD19-mediated CAR activation, PMA stimulation, and ionomycin

Figure 4. Combinatorial targets differentially decode temporal TF interactions

- (A) The design of RNA-seq experiments for profiling the effect of temporal TF interactions on combinatorial target genes. RNA-seq experiments under PMA-only or ionomycin-only stimulation were also performed. Note that the identified genes were a subset of genes from Figure S1D. See Figure S8A for details.
 - (B) Cartoons illustrating the calculation of effect size of the TF interaction on each gene (STAR Methods).
 - (C) Pearson correlations of the effect sizes (log2 transformed) under different stimulations, including PMA/ionomycin, TCR, and CAR activation. The ratio between experimentally measured and estimated gene expression levels was calculated as the effect size of TF interactions. n = 58 genes. *p < 0.05, **p < 0.01, ***p < 0.001.
 - (D) Scatterplots comparing the effect sizes (log2 transformed) of combinatorial target genes between the TCR activation condition and different CAR activation conditions. Note that Pearson correlations were calculated for data like these and are summarized in (C). n = 58 genes.
 - (E) Heatmap showing that combinatorial target genes can be clustered into two groups based on the effect sizes under various stimulations. Hierarchical clustering was performed using the ward.D method based on Euclidean distance. There are 8 genes in group 1 and 50 genes in group 2.
 - (F) Results from GO analysis of the two gene groups in (E).
- See also Figure S7 and S8.

stimulation. The latter two conditions would measure how individual pathway TFs (NF- κ B or NFAT) regulate gene expression, allowing us to quantify gene regulation in the absence of temporal pathway integration and to compare it with the first two conditions where both TFs are activated (Figures 4A and S7A).

To decipher the role of temporal pathway integration (via the interactions of the two TFs) on target gene regulation, we needed to infer the effect size of TF interactions on each gene. To do so, we calculated the fold change between experimentally measured gene expression changes when both TFs were activated versus hypothetical gene expression changes when assuming additive (and non-synergistic) interactions between the two TFs. To calculate the hypothetical gene expression change, we summed the scaled gene expression changes measured under conditions where only one TF was activated (i.e., PMA only and ionomycin only), where the scaling factor was calculated using the ratio of TF activities between the condition with both TFs activated and the condition with only one TF activated (STAR Methods). The rationale for such a calculation is that gene expression levels under PMA-only and ionomycin-only conditions can be used to estimate the quantitative effects of each TF on gene expression under other conditions when assuming the absence of interactions between TFs. Thus, the estimated effect size, quantified as the measured expression change divided by the hypothetical expression change when assuming non-synergistic interactions, allowed us to estimate the extent of the TF interactions on different target genes (Figure 4B; STAR Methods).

By profiling the effect sizes of TF interactions on individual genes across conditions, we found that the effect sizes are significantly correlated between conditions (Figures 4C and 4D; Table S2). This result implied that the effect sizes of different genes are partially determined in *cis*, where the *cis*-regulatory sequences greatly affect how the two TFs interact to regulate corresponding genes. Importantly, across conditions, we consistently observed a group of genes that were synergistically upregulated by the two TFs (Figure 4E, top; Table S2), where the temporal TF interactions appear to confer higher expression increases in a cooperative manner (compared with when regulated by the two TFs in an additive manner). In contrast, we also consistently observed a second group of genes that were relatively downregulated compared with additive regulation (Figure 4E, bottom).

Functionally, the first group of genes is significantly enriched for critical T cell functions (Figure 4F), including cell-cell adhesion and immune effector process, while the Gene Ontology (GO) term with the largest number of genes for the second group relates to the negative regulation of immune response. These results suggest a potential role of temporal TF interactions in conferring cooperative immune gene regulation. Of note, the effect size quantified the synergistic effect of the two TFs on target genes instead of the fold activation of the target genes, and thus the fold change of the first group of genes may not necessarily be higher than that of the second group (Figures S7B and S7C).

Further characterization of the *cis*-regulatory regions of two gene groups suggested potential *cis*-regulatory features that might be associated with the distinct regulatory outcomes (Figures S7D and S7E). We thus sought to compare the chro-

matin accessibility of regulatory regions between the two gene groups. To do so, we performed assay for transposase-accessible chromatin with high-throughput sequencing (ATAC-seq) measurements on Jurkat T cells along the time course of the treatment of PMA only, ionomycin only, or PMA/ionomycin (Figure S7F). By comparing the chromatin accessibility dynamics of the regulatory regions (Figure S7G; STAR Methods), we found, as expected, that co-targets of NFAT and NF- κ B exhibited markedly enhanced chromatin accessibility when both pathways were activated by PMA/ionomycin compared with when only one pathway was activated (Figure S7H). Moreover, co-target genes whose gene expression levels were upregulated in response to PMA/ionomycin stimulation (a total of 130 genes) displayed further enhanced promoter accessibility (Figure S7I). We next compared the changes in accessibility between the two gene groups above and found that, while their accessibility was enhanced by co-activation of the two pathways, no difference was observed in fold change (Figure S7J), suggesting a perplexing nature of the observed synergy between the two TFs. The potential involvement of hidden factors that could contribute to the observed effects remains to be further investigated.

Nevertheless, these results demonstrated that quantitative principles identified in TCR signaling are likely shared by CAR signaling and that the temporal relationship between NFAT and NF- κ B allows fine-tuning the extent of combinatorial regulation during T cell activation mediated by natural and artificial receptors.

Dynamic combinatorial regulation of synthetic promoters

While the two TFs appear to temporally interact to synergistically regulate endogenous targets, it remains unclear whether such regulation would depend on *cis*-regulatory elements other than the binding sites of the two TFs. To address this, we resorted to synthetic reporters with rationally designed TF binding configurations.⁴⁷

We constructed a monoclonal cell line with a synthetic reporter containing four copies of the binding motif of each TF, driving expression of mCitrine or mTurquoise2, as well as a combinatorial reporter comprising both binding motifs, driving expression of mCherry (Figure S8A). Using this cell line, we could ask whether the effect size of temporal TF interactions on the synthetic reporter would resemble that of the endogenous genes. We thus subjected cells to a range of PMA/ionomycin conditions, allowing us to measure the responses of the synthetic reporter to activation of one or both TFs. Based on these data, we found that activation of both TFs synergistically upregulated expression of the reporter gene (Figure S8B). To further explore the effect of binding motif arrangement, we constructed a second cell line with a different combinatorial reporter by swapping the binding cassettes of NFAT and NF- κ B. We observed analogous effect sizes despite binding cassette swapping (Figure S8C). Together, these results suggested that the presence of both binding sites is sufficient to confer the synergistic regulatory effects between activated NFAT and NF- κ B. It would be helpful to further perturb the temporal dynamics and characterize the influence on effect size using synthetic reporters.

DISCUSSION

Deciphering the regulatory principles of T cell response genes is critical for decoding and engineering immunity and has been impeded by complex *cis*-regulatory schemes, where multiple pathways integrate through combinatorial binding of terminal TFs. This task is further complicated because key TFs involved in T cell response have been shown to display intricate temporal activity dynamics. Our results suggest that NFAT and NF- κ B display significant co-binding to T cell response genes and that their temporal relationships are modulated mostly in an analog manner, enabling differential target gene regulation during TCR or CAR signaling. This work thus sheds light on how different pathways in human T cells can combinatorially interact in a temporal manner to regulate immune response, adding to the growing list of signaling systems where the signaling responses are regulated by multiple dynamic factors that interact temporally.^{14,17,26,48}

We illustrated two fundamental elements of dynamic combinatorial gene regulation. First, the upstream regulators should exhibit a higher-than-random potential of physical interactions in the *cis*-regulatory regions of co-targets. Importantly, co-binding of TFs to the same target genes could arise from random coincidence, and the availability of genome-wide binding profiles enabled us to discriminate between a passive versus active mode of co-binding. Second, the upstream regulators should interact dynamically, reflected by temporally coordinated co-activation or correlated activity levels. It should be noted that temporal interactions could also occur through modulation of the relative timing of activity pulses in individual cells^{14,17,26} or through sequential binding events.¹⁸

It is intriguing that TCR signaling and CAR signaling appear to share similar principles for dynamic combinatorial regulation of immune response genes by NFAT and NF- κ B. More specifically, when a TCR or CAR is bound with antigen, T cells would actively modulate the temporal relationships between the two TFs in an analog manner, leading to synergistic regulatory effects on target genes. We identified a group of genes, most enriched for positive immune-regulatory functions, being cooperatively regulated during this process, while another group of genes, most enriched for negative immune-regulatory functions, being oppositely regulated. This finding suggests a conserved dynamic gene-regulatory mechanism that accounts for different modes of regulatory outcomes for genes within distinct functional groups.

Mechanistic insights into natural T cell signaling can help to engineer synthetic receptors such as CARs. We found that the three anti-CD19 CARs (i.e., ζ , 28- ζ , and BB- ζ CAR) exhibited differential NFAT and NF- κ B signaling dynamics in Jurkat and primary human T cells, where signaling through BB- ζ CAR mediated the strongest activation of both TFs and modulated their temporal relationships to achieve synergistic gene regulation. Because CAR signaling is mediated by dynamic combinatorial principles analogous to TCR signaling, mechanisms found to modulate TCR signaling could be incorporated as control knobs for tuning CAR signaling, such as mechanisms influencing the dynamic interplay between NFAT and NF- κ B.

Limitations of the study

For the characterization of temporal TF dynamics, we focused on comparing the population-averaged (instead of single-cell-level) effects of temporal TF interactions between genes and across conditions. Mechanistically, while a *cis*-regulatory mechanism likely contributes to the decoding of TF temporal relationships by downstream genes, we did not find supporting evidence from the analysis of chromatin accessibility. It is likely that the *cis*-regulatory structure plays a role in the decoding process by recruiting additional factors. To apply findings from this study to the design of synthetic receptors such as CARs, it would be helpful to include additional variants of CAR designs and more systematically map the relationship between temporal pathway dynamics and the sequences of synthetic receptors.

STAR★METHODS

Detailed methods are provided in the online version of this paper and include the following:

- [KEY RESOURCES TABLE](#)
- [RESOURCE AVAILABILITY](#)
 - Lead contact
 - Materials availability
 - Data and code availability
- [EXPERIMENTAL MODEL AND STUDY PARTICIPANT DETAILS](#)
 - Cell lines
- [METHOD DETAILS](#)
 - Cell culture
 - Plasmid construction
 - Lentivirus production
 - T cell activation
 - Live-cell imaging
 - Imaging data analysis
 - Quantification of digital modulation
 - Cross-correlation analysis
 - RNA-seq
 - ATAC-seq
 - Bioinformatic analysis
- [QUANTIFICATION AND STATISTICAL ANALYSIS](#)

SUPPLEMENTAL INFORMATION

Supplemental information can be found online at <https://doi.org/10.1016/j.celrep.2023.112663>.

ACKNOWLEDGMENTS

We thank the Flow Cytometry Core at the National Center for Protein Sciences at PKU, the Quantitative Imaging Facility at the CQB, and the High-Performance Computing Platform at the CLS for equipment support. This work was supported by grants from the National Key R&D Program of China (2018YFA0900703, 2019YFA09004500, and 2020YFA0906900), the Strategic Priority Research Program of the Chinese Academy of Sciences (XDB04800000), and the National Natural Science Foundation of China (32088101 and 31771425). We thank Dr. Wendell Lim, Dr. Arthur Weiss, and Dr. Haopeng Wang for the gifts of plasmids/cell lines.

AUTHOR CONTRIBUTIONS

Conceptualization, P.W., Y.L., and W.H.; methodology, W.H., B.C., and J.Z.; investigation, W.H., W.L., Y.L., and P.W.; writing – original draft, W.H. and Y.L.; writing – review & editing, W.H., Y.L., and P.W.; funding acquisition, P.W. and Y.L.; resources, P.G. and Y.F.; supervision, P.W. and Y.L.

DECLARATION OF INTERESTS

The authors declare no competing interests.

Received: August 4, 2022

Revised: April 2, 2023

Accepted: June 2, 2023

Published: June 21, 2023

REFERENCES

1. Smith-Garvin, J.E., Koretzky, G.A., and Jordan, M.S. (2009). Cell activation. *Annu. Rev. Immunol.* **27**, 591–619.
2. Koch, U., and Radtke, F. (2011). Mechanisms of T Cell development and transformation. *Annu. Rev. Cell Dev. Biol.* **27**, 539–562.
3. Chen, L., and Flies, D.B. (2013). Molecular mechanisms of T cell co-stimulation and co-inhibition. *Nat. Rev. Immunol.* **13**, 227–242.
4. Berry, C.T., May, M.J., and Freedman, B.D. (2018). STIM- and Orai-mediated calcium entry controls NF-κB activity and function in lymphocytes. *Cell Calcium* **74**, 131–143.
5. Cheng, J., Montecalvo, A., and Kane, L.P. (2011). Regulation of NF-κB induction by TCR/CD28. *Immunol. Res.* **50**, 113–117.
6. Trebak, M., and Kinet, J.-P. (2019). Calcium signalling in T cells. *Nat. Rev. Immunol.* **19**, 154–169.
7. Neelapu, S.S., Tummala, S., Kebrabaei, P., Wierda, W., Gutierrez, C., Locke, F.L., Komanduri, K.V., Lin, Y., Jain, N., Daver, N., et al. (2018). Chimeric antigen receptor T-cell therapy — assessment and management of toxicities. *Nat. Rev. Clin. Oncol.* **15**, 47–62.
8. Larson, R.C., and Maus, M.V. (2021). Recent advances and discoveries in the mechanisms and functions of CAR T cells. *Nat. Rev. Cancer* **21**, 145–161.
9. Brudno, J.N., and Kochenderfer, J.N. (2018). Chimeric antigen receptor T-cell therapies for lymphoma. *Nat. Rev. Clin. Oncol.* **15**, 31–46.
10. Salter, A.I., Rajan, A., Kennedy, J.J., Ivey, R.G., Shelby, S.A., Leung, I., Templeton, M.L., Muhunthan, V., Voillet, V., Sommermeyer, D., et al. (2021). Comparative analysis of TCR and CAR signaling informs CAR designs with superior antigen sensitivity and in vivo function. *Sci. Signal.* **14**, eabe2606.
11. Ravasi, T., Suzuki, H., Cannistraci, C.V., Katayama, S., Bajic, V.B., Tan, K., Akalin, A., Schmeier, S., Kanamori-Katayama, M., Bertin, N., et al. (2010). An atlas of combinatorial transcriptional regulation in mouse and man. *Cell* **140**, 744–752.
12. Gerstein, M.B., Kundaje, A., Hariharan, M., Landt, S.G., Yan, K.K., Cheng, C., Mu, X.J., Khurana, E., Rozowsky, J., Alexander, R., et al. (2012). Architecture of the human regulatory network derived from ENCODE data. *Nature* **489**, 91–100.
13. Han, H., Cho, J.W., Lee, S., Yun, A., Kim, H., Bae, D., Yang, S., Kim, C.Y., Lee, M., Kim, E., et al. (2018). TRRUST v2: an expanded reference database of human and mouse transcriptional regulatory interactions. *Nucleic Acids Res.* **46**, D380–D386.
14. Lin, Y., Sohn, C.H., Dalal, C.K., Cai, L., and Elowitz, M.B. (2015). Combinatorial gene regulation by modulation of relative pulse timing. *Nature* **527**, 54–58.
15. Levine, J.H., Lin, Y., and Elowitz, M.B. (2013). Functional roles of pulsing in genetic circuits. *Science* **342**, 1193–1200.
16. Yissachar, N., Sharar Fischler, T., Cohen, A.A., Reich-Zeliger, S., Russ, D., Shifrut, E., Porat, Z., and Friedman, N. (2013). Dynamic response diversity of NFAT isoforms in individual living cells. *Mol. Cell* **49**, 322–330.
17. Wu, Y., Wu, J., Deng, M., and Lin, Y. (2021). Yeast cell fate control by temporal redundancy modulation of transcription factor paralogs. *Nat. Commun.* **12**, 3145.
18. Cheng, C.S., Behar, M.S., Suryawanshi, G.W., Feldman, K.E., Spreafico, R., and Hoffmann, A. (2017). Iterative modeling reveals evidence of sequential transcriptional control mechanisms. *Cells* **4**, 330–343.e5.
19. Purvis, J.E., and Lahav, G. (2013). Encoding and decoding cellular information through signaling dynamics. *Cell* **152**, 945–956.
20. Hao, N., and O'Shea, E.K. (2011). Signal-dependent dynamics of transcription factor translocation controls gene expression. *Nat. Struct. Mol. Biol.* **19**, 31–39.
21. Purvis, J.E., Karhohs, K.W., Mock, C., Batchelor, E., Loewer, A., and Lahav, G. (2012). p53 dynamics control cell fate. *Science* **336**, 1440–1444.
22. Selimkhanov, J., Taylor, B., Yao, J., Pilko, A., Albeck, J., Hoffmann, A., Tsimring, L., and Wollman, R. (2014). Accurate information transmission through dynamic biochemical signaling networks. *Science* **346**, 1370–1373.
23. Hansen, A.S., and O'Shea, E.K. (2015). Limits on information transduction through amplitude and frequency regulation of transcription factor activity. *Elife* **4**, e06559.
24. Nandagopal, N., Santat, L.A., LeBon, L., Sprinzak, D., Bronner, M.E., and Elowitz, M.B. (2018). Dynamic ligand discrimination in the notch signaling pathway. *Cell* **172**, 869–880.e19.
25. Zhang, Q., Gupta, S., Schipper, D.L., Kowalczyk, G.J., Mancini, A.E., Faeber, J.R., and Lee, R.E.C. (2017). NF-κB dynamics discriminate between TNF doses in single cells. *Cell Syst.* **5**, 638–645.e5.
26. Sonnen, K.F., Lauschke, V.M., Uraji, J., Falk, H.J., Petersen, Y., Funk, M.C., Beaupex, M., François, P., Merten, C.A., and Aulehla, A. (2018). Modulation of phase shift between Wnt and notch signaling oscillations controls mesoderm segmentation. *Cell* **172**, 1079–1090.e12.
27. Zhang, Z.-B., Wang, Q.Y., Ke, Y.X., Liu, S.Y., Ju, J.Q., Lim, W.A., Tang, C., and Wei, P. (2017). Design of tunable oscillatory dynamics in a synthetic NF-κB signaling circuit. *Cell Syst.* **5**, 460–470.e5.
28. Nelson, D.E., Ihekweazu, A.E.C., Elliott, M., Johnson, J.R., Gibney, C.A., Foreman, B.E., Nelson, G., See, V., Horton, C.A., Spiller, D.G., et al. (2004). Oscillations in NF-κB signaling control the dynamics of gene expression. *Science* **306**, 704–708.
29. Tay, S., Hughey, J.J., Lee, T.K., Lipniacki, T., Quake, S.R., and Covert, M.W. (2010). Single-cell NF-κB dynamics reveal digital activation and analog information processing in cells. *Nature* **466**, 267–271.
30. Buchler, N.E., Gerland, U., and Hwa, T. (2003). On schemes of combinatorial transcription logic. *Proc. Natl. Acad. Sci. USA* **100**, 5136–5141.
31. Oki, S., Ohta, T., Shioi, G., Hatanaka, H., Ogasawara, O., Okuda, Y., Kawaji, H., Nakaki, R., Sese, J., and Meno, C. (2018). A data-mining suite powered by full integration of public ChIP-seq data. *EMBO Rep.* **19**, e46255.
32. Marangoni, F., Murooka, T.T., Manzo, T., Kim, E.Y., Carrizosa, E., Elpek, N.M., and Mempel, T.R. (2013). The transcription factor NFAT exhibits signal memory during serial T cell interactions with antigen-presenting cells. *Immunity* **38**, 237–249.
33. Maguire, O., O'Loughlin, K., and Minderman, H. (2015). Simultaneous assessment of NF-κB/p65 phosphorylation and nuclear localization using imaging flow cytometry. *J. Immunol. Methods* **423**, 3–11.
34. Müller, M.R., and Rao, A. (2010). Immunity and cancer: a transcription factor comes of age. *Nat. Rev. Immunol.* **10**, 645–656.
35. Aron, J.R., Winslow, M.M., Polleri, A., Chang, C.P., Wu, H., Gao, X., Neilson, J.R., Chen, L., Heit, J.J., Kim, S.K., et al. (2006). NFAT dysregulation by increased dosage of DSCR1 and DYRK1A on chromosome 21. *Nature* **441**, 595–600.

36. Beals, C.R., Sheridan, C.M., Turck, C.W., Gardner, P., and Crabtree, G.R. (1997). Nuclear export of NF-ATc enhanced by glycogen synthase kinase-3. *Science* 275, 1930–1934.
37. Inoue, K., Shinohara, H., Behar, M., Yumoto, N., Tanaka, G., Hoffmann, A., Aihara, K., and Okada-Hatakeyama, M. (2016). Oscillation dynamics underlie functional switching of NF-κB for B-cell activation. *NPJ Syst. Biol. Appl.* 2, 16024–16029.
38. Lee, T.K., Denny, E.M., Sanghvi, J.C., Gaston, J.E., Maynard, N.D., Hughey, J.J., and Covert, M.W. (2009). A noisy paracrine signal determines the cellular NF-κB response to lipopolysaccharide. *Sci. Signal.* 2, ra65.
39. Alves, B.N., Tsui, R., Almaden, J., Shokhirev, M.N., Davis-Turak, J., Fujimoto, J., Birnbaum, H., Ponomarenko, J., and Hoffmann, A. (2014). IκBε is a key regulator of B cell expansion by providing negative feedback on cRel and RelA in a stimulus-specific manner. *J. Immunol.* 192, 3121–3132.
40. Sun, S.-C. (2017). The non-canonical NF-κB pathway in immunity and inflammation. *Nat. Rev. Immunol.* 17, 545–558.
41. Palkowitsch, L., Marienfeld, U., Brunner, C., Eitelhuber, A., Krappmann, D., and Marienfeld, R.B. (2011). The Ca²⁺-dependent phosphatase calcineurin controls the formation of the carma1-Bcl10-malt1 complex during T cell receptor-induced NF-κB activation. *J. Biol. Chem.* 286, 7522–7534.
42. Toeplitz, B.K., Cohen, A.I., Funke, P.T., Parker, W.L., and Gougoutas, J.Z. (1979). Structure of ionomycin - a novel diacidic polyether antibiotic having high affinity for calcium ions. *J. Am. Chem. Soc.* 101, 3344–3353.
43. Touraine, J.L., Hadden, J.W., Touraine, F., Hadden, E.M., Estensen, R., and Good, R.A. (1977). Phorbol myristate acetate: a mitogen selective for a T-lymphocyte subpopulation. *J. Exp. Med.* 145, 460–465.
44. Liu, D., Badeti, S., Dotti, G., Jiang, J.G., Wang, H., Dermody, J., Soteropoulos, P., Streck, D., Birge, R.B., and Liu, C. (2020). The role of immunological synapse in predicting the efficacy of chimeric antigen receptor (CAR) immunotherapy. *Cell Commun. Signal.* 18, 134.
45. Rydzek, J., Nerreter, T., Peng, H., Jutz, S., Leitner, J., Steinberger, P., Einsele, H., Rader, C., and Hudecek, M. (2019). Chimeric antigen receptor library screening using a novel NF-κB/NFAT reporter cell Platform. *Mol. Ther.* 27, 287–299.
46. Kawalekar, O.U., O' Connor, R.S., Fraietta, J.A., Guo, L., McGettigan, S.E., Posey, A.D., Jr., Patel, P.R., Guedan, S., Scholler, J., Keith, B., et al. (2016). Distinct signaling of coreceptors regulates specific metabolism pathways and impacts memory development in CAR T cells. *Immunity* 44, 712–730.
47. Jutz, S., Leitner, J., Schmetterer, K., Doel-Perez, I., Majdic, O., Grabmeier-Pfistershammer, K., Paster, W., Huppa, J.B., and Steinberger, P. (2016). Assessment of costimulation and coinhibition in a triple parameter T cell reporter line: simultaneous measurement of NF-κB, NFAT and AP-1. *J. Immunol. Methods* 430, 10–20.
48. AkhavanAghdam, Z., Sinha, J., Tabbaa, O.P., and Hao, N. (2016). Dynamic control of gene regulatory logic by seemingly redundant transcription factors. *Elife* 5, e18458.
49. Kim, D., Langmead, B., and Salzberg, S.L. (2015). HISAT: a fast spliced aligner with low memory requirements. *Nat. Methods* 12, 357–360.
50. Putri, G.H., Anders, S., Pyl, P.T., Pimanda, J.E., and Zanini, F. (2022). Analysing high-throughput sequencing data in Python with HTSeq 2.0. *Bioinformatics* 38, 2943–2945.
51. Heinz, S., Benner, C., Spann, N., Bertolino, E., Lin, Y.C., Laslo, P., Cheng, J.X., Murre, C., Singh, H., and Glass, C.K. (2010). Simple combinations of lineage-determining transcription factors prime cis-regulatory elements required for macrophage and B cell identities. *Mol. Cell* 38, 576–589.
52. Krueger, F., James, F., Ewels, P., Afyounian, E., Weinstein, M., Schuster-Boeckler, B., Hulselmans, G., and Slamons. (2023). FelixKrueger/Trim-Galore: v0.6.10 - add default decompression path. <https://doi.org/10.5281/zenodo.7598955>.
53. Love, M.I., Huber, W., and Anders, S. (2014). Moderated estimation of fold change and dispersion for RNA-seq data with DESeq2. *Genome Biol.* 15, 550.
54. Langmead, B., and Salzberg, S.L. (2012). Fast gapped-read alignment with Bowtie 2. *Nat. Methods* 9, 357–359.
55. Danecek, P., Bonfield, J.K., Liddle, J., Marshall, J., Ohan, V., Pollard, M.O., Whitwham, A., Keane, T., McCarthy, S.A., Davies, R.M., and Li, H. (2021). Twelve years of SAMtools and BCFtools. *GigaScience* 10, giab008.
56. Zhang, Y., Liu, T., Meyer, C.A., Eeckhoute, J., Johnson, D.S., Bernstein, B.E., Nusbaum, C., Myers, R.M., Brown, M., Li, W., and Liu, X.S. (2008). Model-based analysis of ChIP-seq (MACS). *Genome Biol.* 9, R137.
57. Neph, S., Kuehn, M.S., Reynolds, A.P., Haugen, E., Thurman, R.E., Johnson, A.K., Rynes, E., Maurano, M.T., Vierstra, J., Thomas, S., et al. (2012). BEDOPS: high-performance genomic feature operations. *Bioinformatics* 28, 1919–1920.
58. Quinlan, A.R., and Hall, I.M. (2010). BEDTools: a flexible suite of utilities for comparing genomic features. *Bioinformatics* 26, 841–842.

STAR★METHODS

KEY RESOURCES TABLE

REAGENT or RESOURCE	SOURCE	IDENTIFIER
Antibodies		
Ultra-LEAF™ Purified anti-human CD3 (OKT3)	BioLegend	Cat# 317350; RRID: AB_2749889
Ultra-LEAF™ Purified anti-human CD28 (CD28.2)	BioLegend	Cat# 302960; RRID: AB_2800749
Bacterial and virus strains		
<i>trans</i> 5α chemically Competent Cell	Transgen	Cat# CD201-02
Lentivirus	This paper	N/A
Chemicals, peptides, and recombinant proteins		
Poly-D-lysine	Thermo Fisher Scientific	Cat# A3890401
SYTO™ Deep red fluorescent Nucleic Acid stain	Thermo Fisher Scientific	Cat# S34900
Calbryte™ 590 AM	AAT Bioquest	Cat# 20700
NP-40	Sigma	Cat# NP40
Tween®20	Sigma	Cat# P1379
Digitonin	Promega	Cat# G9441
Recombinant human IL-2	Novoprotein	Cat# GMP-CD66
BamHI-HF	New England Biolabs	Cat# R3136L
Ndel	New England Biolabs	Cat# R0111L
NotI	New England Biolabs	Cat# R0189L
Critical commercial assays		
pEASY®-basic Seamless cloning and assembly Kit	Transgen	Cat# CU201-03
QIAprep Spin Miniprep Kit (250)	Qiagen	Cat# 27106
EasySep™ human CD3 positive Selection Kit II	Stemcell	Cat# 17851
TruePrep™ DNA library Prep Kit V2 for Illumina	Vazyme	Cat# TD502
TruePrep™ Index Kit V2 for Illumina	Vazyme	Cat# TD302
VAHTS DNA Clean Beads	Vazyme	Cat# N4
High sensitivity NGS fragment analysis Kit (1bp-6000bp)	Agilent	Cat# DNF-474-0500
Deposited data		
RNA-seq, ATAC-seq data	This paper	Bioproject ID: PRJNA950538 https://www.ncbi.nlm.nih.gov/bioproject?term=PRJNA950538
Code to reproduce the analysis	This paper	https://doi.org/10.5281/zenodo.7948465
Experimental models: Cell lines		
LX293T	Laboratory of Wendell Lim	N/A
K562	Laboratory of Wendell Lim	N/A
Jurkat	Laboratory of Arthur Weiss	N/A
Human PBMC	ALLCELLS	PB004F-C
Recombinant DNA		
Plasmid: α-CD19-CD8a-ζ-T2A-mCherry	This paper	N/A
Plasmid: α-CD19-CD8a-4-1BB-ζ-T2A-mCherry	This paper	N/A
Plasmid: α-CD19-CD8a-CD28-ζ-T2A-mCherry	This paper	N/A
Plasmid: CD19-BFP	This paper	N/A
Plasmid: H2B-iRFP	This paper	N/A
Plasmid: mTurquoise2-NFAT1	This paper	N/A
Plasmid: RelA-mCitrine	This paper	N/A
Plasmid: p-NFAT-mCitrine	This paper	N/A
Plasmid: p-NFKB-mTurquoise2	This paper	N/A

(Continued on next page)

Continued

REAGENT or RESOURCE	SOURCE	IDENTIFIER
Software and algorithms		
Fiji	NIH	https://imagej.net/Fiji/Download
Imaris 9.2.1	Oxford instruments	https://imaris.oxinst.com/support/imaris-release-notes/9-2-0
FlowJo	BD Biosciences	https://www.flowjo.com/
MATLAB2017b	Mathworks	https://www.mathworks.com/products/matlab.html
R (version 4.0.2)	The R Foundation	https://www.r-project.org/
Hisat2	Kim et al. ⁴⁹	https://daehwankimlab.github.io/htseq2/
HTseq	Putri et al. ⁵⁰	https://htseq.readthedocs.io/en/master/
Homer	Heinz et al. ⁵¹	http://homer.ucsd.edu/homer/
Trim galore	Krueger et al. ⁵²	https://github.com/FelixKrueger/TrimGalore
DESeq2	Love et al. ⁵³	https://bioconductor.org/packages/release/bioc/html/DESeq2.html
Bowtie2	Langmead et al. ⁵⁴	https://bowtie-bio.sourceforge.net/bowtie2/index.shtml
SAMtools	Danecek et al. ⁵⁵	https://github.com/samtools/samtools
Macs2	Zhang et al. ⁵⁶	https://pypi.python.org/pypi/MACS2/
Bedops	Neph et al. ⁵⁷	https://github.com/bedops/bedops
Bedtools	Quinlan et al. ⁵⁸	https://bedtools.readthedocs.io/en/latest/

RESOURCE AVAILABILITY

Lead contact

Further information and requests for resources and reagents should be directed to and will be fulfilled by the lead contact, Yihan Lin (yihan.lin@pku.edu.cn).

Materials availability

Plasmids and cell lines generated in this paper will be shared by the [lead contact](#) upon request.

Data and code availability

- RNA-seq and ATAC-seq data reported in this paper have been deposited at GEO and are publicly available as of the date of publication. The accession number is listed in the [key resources table](#). Microscopy data reported in this paper will be shared by the [lead contact](#) upon request.
- All original code has been deposited at Zenodo and is publicly available as of the date of publication. DOI is listed in the [key resources table](#).
- Any additional information required to reanalyze the data reported in this paper is available from the [lead contact](#) upon request.

EXPERIMENTAL MODEL AND STUDY PARTICIPANT DETAILS

Cell lines

All the cell lines in this work were constructed by lentivirus integration. Jurkat cell line with pNFAT-EGFP and K562 with CD19-BFP were gifts from Arthur Weiss (UCSF). The pNFAT-mCitrine and pNF-κB-mTurquoise2 were constructed and separately integrated into Jurkat cell. We combined the cloned NFAT binding sites from the pNFAT-EGFP plasmid and the NF-κB binding sites before a mini-CMV promoter to generate an NFAT and NF-κB co-target gene reporter (pNFAT-NFKB). Therefore, we generated a dual reporter cell line expressing NFAT, NF-κB targets, and a triple reporter cell line expressing an extra co-target gene. The dual reporter cell line was also transfected with CARs for further characterization in CAR-T cell activation experiments.

The Jurkat cell line for live-cell imaging overexpresses NFAT1-mCitrine, RelA-mTurquoise2 and H2B-iRFP, which was generated by stepwise lentivirus infection. The mono-clones used for both live-cell imaging and FACS tests were sorted by Sony FACS sorter (LE-SH800SFP) or dilution, and screened by α-CD3 and α-CD28 (BioLegend) stimulation. To select for mono-clone used for imaging,

we looked for clones showing low basal expression and an obvious nuclear translocation under stimulation. For the reporter cell line, we looked for clones showing up-regulated downstream fluorescent protein expression and a low basal level in the rested state.

Before lentivirus infection, primary CD3+ cells were activated for expansion in α -CD3/ α -CD28 antibodies (1 μ g/mL) pre-coated plates for 48 h. Primary CD3+ CAR-T cells were infected by lentivirus for constructing α -CD19 CAR-T cells for live-cell imaging, which also overexpressed NFAT1-mCitrine, RelA-mTurquoise2, as well as mCherry fused CAR. Before imaging, triple-positive CAR-T cells were FACS sorted and incubated with SYTO Deep Red Fluorescent Nucleic Acid Stain dye for nuclear labeling.

METHOD DETAILS

Cell culture

293LX cells were cultivated in Dulbecco's Modified Eagle Medium (DMEM, Gibco) supplemented with 10% fetal bovine serum (HyClone) and 1% penicillin-streptomycin (Gibco). Jurkat T cells (ATCC, Clone E6-1), K562 cells and human peripheral blood mononuclear cells (purchased from ALLCELLS) were cultured in basic RPMI-1640 Medium (Gibco) which also supplemented with 10% fetal bovine serum (Gemcell) and 1% penicillin-streptomycin. All cells were cultured at a concentration between 5×10^5 and 5×10^6 cells/mL in a humidity-controlled incubator at 37°C and 5% CO₂. The CD3+ positive T cells were separated from human PBMC after cell recovery by EasySep Human CD3 Positive Selection Kit II and a DPBS buffer containing 2% FBS and 1 mM EDTA.

Plasmid construction

NFAT1 and RelA coding sequences were cloned from human cDNA. The CAR structures were described in the main text. These sequences of interest were inserted into a pHR-SFFV backbone for lentivirus production. The pEASY-Basic Seamless Cloning and Assembly Kit (Transgen) were used for backbone plasmids digestion at NotI/BamHI sites. All plasmids were constructed by Gibson assembly and verified by Sanger sequencing (RUIBO). Plasmids were replicated in DH5 α cells (CWBIOL) using standard protocols. The constructed plasmids were then used for lentivirus production to facilitate the establishment of cell lines. Plasmid maps are available upon request.

Lentivirus production

Plasmids for transfection and lentivirus production were extracted by the QIAprep Spin Miniprep Kit (Qiagen) according to the manufacturer's protocol. We used calcium phosphate to help the transfection of virus-package plasmids PCMVdR8.91 (2.66 μ g), PMD2.G (0.34 μ g) and aimed plasmid (3 μ g) into 293LX cells per well (6-well plate). The transfection medium was replaced with fresh medium 8–10 h after transfection. The supernatant containing lentivirus was harvested 48 h after transfection and centrifuged at 500x g for 5 min to remove cellular debris. Lentiviral particles were subsequently used or aliquoted and frozen at –80°C. All lentivirus infection processes were maintained for 12–24 h before changing fresh cultural medium.

T cell activation

To activate Jurkat T cells, a final concentration of 1 μ g/mL α CD3 and α CD28 were used for the TCR activation at a cell concentration around $0.8\text{--}1 \times 10^6$ /mL. The activation of CAR-T cells, established based on Jurkat T cells, were conducted by the surface-expressed CD19 on K562 cells at a cell number ratio of 1:1. For reporter gene analysis, cells were fixed with a final concentration of 2% PFA at specific time points and detected by LSRFortessaTM flow cytometer (BD Biosciences) and FACSDiva software. Data were compensated and analyzed using FlowJo Software (Tree Star).

Live-cell imaging

For imaging, the glass-bottom plates (Eppendorf or Cellvis, Cell Imaging Plate, 96-well) were pre-treated by 0.5 mg/mL poly-D-lysine (Gibco) for at least 30 min at 37°C or 4°C overnight. The plate was washed twice by DPBS (Gibco) before use. Then $8 \times 10^5\text{--}1 \times 10^6$ T Cells were seeded per well with 100 μ L culture media. After a brief 30 s centrifugation at 10x g, the plate was incubated at 37°C for over 30 min before imaging.

Time-lapse imaging was performed on a Dragonfly 200 High-Speed Confocal Platform (ANDOR) equipped with a CO₂ microscope stage incubator under 5% CO₂ and warmed (37°C) humidified air. We conducted a multi-point, time-lapse imaging controlled by Imaris 9.2.1 with a 5-min time interval for at least 4 h. Designated stimulation was added at t = 0 h and maintained throughout the experimental time course. Images were captured by a Plan-Apo 40x/0.85 objective (Leica) and an Andor Zyla sCMOS camera. The fluorescent protein signals can be separately filtered by CFP filter (478/37, for mTurquoise2), YFP filter (521/38, for mCitrine), RFP filter (594/43, for mCherry), and Cy5 filter (698/77, for iRFP).

Multiple positions within the view were selected before stimulation and the imaging procedure. For experiments monitoring nuclear translocation dynamics of TFs, we added to the culture medium an equal volume of 2x α CD3 and α CD28 antibody premix, reaching a final concentration at 1 μ g/mL. For experiments with calcium imaging, Calbryte 590 AM probe at a final concentration of 1 μ M was added before cell plating, and the medium was changed and resuspended after incubation in the incubator for 1 h.

To monitor CAR-T cell (both Jurkat CAR-T and human primary CAR-T) activation, we pre-seeded 4×10^5 CAR-T cells per well and performed a fast centrifugation as above. The CD19-K562 target cells were added to the well and quickly centrifuged at 10x g for 30 s before imaging.

Imaging data analysis

The images obtained by Dragonfly 200 were all in IMS format and needed to be converted into tiff format files with Fiji. Subsequently, the time-series data (up to 240 min) were segmented and tracked according to the nuclear labeling fluorescence and confirmed by MATLAB. Single-cell traces were extracted based on cell tracking performed on nuclear labeling (i.e., H2B-iRFP). To quantify the response of transcription factors, mean nuclear and cytoplasmic fluorescence intensities in each channel were used for calculating nuclear to cytoplasmic ratio (N/C ratio). Outlier removal (hampel function in MATLAB) and smoothing (sgolayfilt function in MATLAB) were applied to single-cell traces of N/C ratio. Subsequent analyses of single-cell data were performed by R, including the calculation of area under curve of NFAT and NF- κ B nuclear translocation dynamics within the first 4-h of responses (i.e., AUC). It should be noted that we typically pooled single cells from multiple days of experiments together, as many of our analyses (such as the analysis on the temporal relationship) require a relatively large number of cells to obtain statistically significant conclusions. More specifically, for experiments with Jurkat cells under TCR stimulation by α CD3/ α CD28 antibodies, single cells from 4 to 10 different experiments were pooled together. For experiments with Jurkat CAR-T cells, single cells from two experiments were pooled together. For experiments with primary CAR-T cells, single cells from two experiments were pooled together, except for the primary cells with ζ -CAR (only one experiment).

Quantification of digital modulation

Digital modulation was used to quantify whether the co-activation of two TFs occurred more frequently than would be expected by random co-occurrence. To quantify digital modulation, we performed the following steps: 1) We identified cells in which both TFs were activated (i.e., responders) based on predefined activation thresholds for each TF. These thresholds were determined by analyzing the distribution of activation levels in our experimental dataset. More specifically, a single cell was defined as a positive 'NFAT responder' when its NFAT AUC was higher than the maximal AUC of the cell population without treatment. The identification of an 'NF- κ B responder' was based on two metrics: a) the standard deviation of the signal within 90 min of stimulation needs to be above the maximal standard deviation of the cell population without treatment; b) the maximal signal needs to be reached within 90 min of stimulation; 2) We quantified the experimentally observed co-activation fraction by calculating the ratio of responders to the total number of cells; 3) We also calculated the fraction of co-activated cells that would be expected if the two TFs were activated completely independently of each other. This was done by multiplying the individual activation probabilities for each TF; 4) To obtain the digital modulation metric, we divided the observed co-activation fraction by the expected co-activation fraction. A value of one for this metric indicates that there is no digital modulation, implying that the co-activation of the two TFs is random.

Cross-correlation analysis

Cross-correlation of trajectories refers to the analysis of the relationship between the temporal dynamics of two TFs in the same cell. By calculating the cross-correlation between the nuclear localization trajectories of the two TFs, we can assess the degree of synchronization or coordination in their activation patterns over time. A high cross-correlation value at a specific time lag indicates that the two TFs exhibit similar dynamics with a consistent temporal offset, suggesting a potential regulatory relationship between them. In our results of [Figure S2E](#), maximal cross-correlation was at time lag of \sim -5min, indicating that the two TFs display a consistent \sim 5 min delay across different levels of simulations.

RNA-seq

The RNA-seq samples involved in this work were collected using wild-type Jurkat T cells under different stimulations, including PMA, Ionomycin, PMA&Ionomycin, α -CD3& α -CD28 antibody, and different CAR-T cells (constructed based on wild-type Jurkat) with and without stimulation. All samples were stimulated for 4 h.

For RNA-seq experiments, cells were plated at a density of 2×10^6 cells/mL in 1 mL media and rested for 30 min before stimulation in non-tissue culture treated plastic 6-well plates. CAR-T cells were cultured with α -CD19 K562 target cells and sorted by Sony FACS sorter according to the CAR-fused fluorescent protein. Each condition included two replicates. Each replicate contained about $1-5 \times 10^6$ cells, and after stimulation cells were gently mixed with 0.5 mL TRIzol (Invitrogen) for lysing. The sequencing was performed by Illumina NovaSeq 6000 instrument in PE150 mode. Both RNA extraction, library construction, and sequencing were conducted by GeneWiz.

For bulk RNA-seq analysis, quality control of raw data was performed by FastQC (version 0.11.9). The adapters were trimmed by Trim_galore (version 0.6.6) with a parameter: -q 20 -phred33 -stringency 3 -length 20 -e 0.1 -paired. Quality control was performed again on the data after adapter removal. The subsequent sequence alignment process was performed using Hisat2 (version 2.0.1) with hg38 as the reference genome. HTseq (version 0.6.1) was used for the expression analysis. The differential expression levels of each gene were analyzed by DESeq2 (version 1.26.0). We used up-regulated genes with $\log_{2}FC > 0$ for further co-target gene analysis. Gene Ontology analysis was performed by Metascape (<https://metascape.org/>).

ATAC-seq

Stimulated or non-stimulated Jurkat T cells were used to prepare bulk ATAC-seq library. An amount of \sim 50,000 cells were used for library construction, carried out using a TruePrep DNA Library Prep Kit V2 for Illumina (Vazyme) with a standard protocol. Buffer A contains 1M Tris-HCl (pH = 7.4), 5M NaCl, and 1M MgCl₂, based on which the cell lysis buffer was made by adding 0.1% NP-40,

0.1% Tween 20, and 0.01% digitonin. The VAHTS DNA Clean Beads (Vazyme) were used for DNA fragments purification. All the DNA libraries passed quality control (performed using a High Sensitivity NGS Fragment Analysis Kit on a Agilent 2100 Bioanalyzer) before pair-end sequencing of 150 bp using HiSeq (Illumina).

All bulk ATAC-seq data were trimmed using Trim_galore (version 0.6.6) with the “q 20 -phred33 -stringency 3 -length 20 -e 0.1 -paired” option and aligned to the human reference genome (hg38) using Bowtie2 (version 2.3.5.1). SAMtools (version 1.10) were used for post-alignment processing, including the removal of low-quality reads, PCR duplicates, and mitochondrial DNA reads, resulting in bam files for peaking finding and chromatin accessibility analysis. The ‘summits’ of all samples produced by macs2 callpeak (version 2.2.7.1, parameter: –shift –100 –extsize 200 –nomodel -B –SPMR -g hs) were extended into 500bp and merged by bedops (version 2.4.38). Raw read counts were extracted by bedtools (version 2.29.1) multicov.

Bioinformatic analysis

We downloaded the predicted target genes bound by given transcription factors from ChIP-Atlas (https://chip-atlas.org/target_genes) and combined results in human CD4+ T cells (including Th1 cells) due to the scarcity of cell-type-specific NFAT ChIP-seq data. The number of co-target genes (weight) and the fold-change between actual and random co-binding-target number were calculated to represent the strength of physical co-binding. The co-regulating relationship of transcription factor pairs calculated by hypergeometric test.

The effect size of TF interactions on each gene was used to describe the degree of TF integration on co-target genes. We calculated the area under curve in N/C ratio traces (0–4 h) to represent the TF activity. Because Ionomycin and PMA can activate NFAT and NF-κB separately, and target gene expression levels were assumed to be closely linked to TF activity, and the TF activity (AUC) and RNA expression level were used to infer hypothetical target gene expression without synergistic TF interaction (Equation 1; using TCR condition as an example). The effect size (Equation 2) was defined as the measured expression change divided by the hypothetical expression change for each co-target gene:

$$RNA_{hyp} = \frac{AUC_{TCR,NFAT}}{AUC_{Iono,NFAT}} \times RNA_{Iono,NFAT} + \frac{AUC_{TCR,NFkB}}{AUC_{PMA,NFkB}} \times RNA_{PMA,NFkB} \quad (\text{Equation 1})$$

$$\text{Effect size} = \frac{RNA_{exp}}{RNA_{hyp}} \quad (\text{Equation 2})$$

For genes classified into two groups in Figure 4, we analyzed the potential NFAT1 or RELA binding sites ±5 kb around the TSS by homer (version 4.11) annotatePeaks.pl. The number of NFAT1 or RELA motif within the same gene was counted, and the minimum distance between potential NFAT1 or RELA binding sites was calculated according to their distances to TSS.

To identify regulatory regions of NFAT and NF-κB co-target genes, we calculated the area under curve (AUC) of each peak annotated to these genes. AUC was calculated using the temporal trace of the fold change compared to unstimulated samples. Putative regulatory regions were chosen by selecting ATAC-seq peaks that exhibited the highest AUC.

QUANTIFICATION AND STATISTICAL ANALYSIS

The data are presented as mean ± s.d. as indicated in the figure legends. For comparisons between groups, the data were analyzed by Welch Two Sample t test. All statistical analyses were performed using R software. The calculated p value are reported using the symbols: ‘n.s.’ denotes non-significant, ‘*’ denotes $p < 0.05$, ‘**’ denotes $p < 0.01$, ‘***’ denotes $p < 0.001$, and ‘****’ denotes $p < 0.0001$.